Hindawi
Advances in Civil Engineering
Volume 2021, Article ID 6677595, 13 pages
https://doi.org/10.1155/2021/6677595

Research Article

Penetration Form of Inter-Hole Cracks under Double-Hole Blasting Conditions with Inclined Fissures

Shiwei Shen,[1] Yue Zhao,[1] Chang Liu ,[1,2] Shulin Dai,[1] Fei Wu,[1] and Man Jiang[1]

[1]*College of Construction Engineering, Jilin University, Changchun, Jilin 130026, China*
[2]*College of Art and Design, Jilin Jianzhu University, Changchun, Jilin 130118, China*

Correspondence should be addressed to Chang Liu; liuchang@jlju.edu.cn

Received 27 October 2020; Revised 29 December 2020; Accepted 7 January 2021; Published 30 January 2021

Academic Editor: Yilin Gui

During blasting construction in tunnel engineering, an inclined fissure near the blast hole produces the "*Z*" type of over-excavation and subsequently affects the overall blasting effect and stability of the tunnel. In this work, dynamic caustics testing was used to study the burst propagation mode and penetration form of explosive cracks at different positions between holes under double-hole blasting conditions. Results showed that the existence of gently inclined cracks changed the propagation law of explosive stress wave. The dominant fracture surface was formed in the vertical direction between the borehole and the fracture. Finally, the crack penetrates to form "*Z*"-type over-excavation, which was analyzed by the dynamic caustics test. The expansion velocity of the burst crack reached the maximum under the reflection of the explosion stress wave and then decreased with the attenuation of the stress wave intensity. The peak propagation velocity decreased with the increasing vertical distance between the prefabricated fracture and the borehole, and the stress intensity factor at the crack tip immediately reached its peak value after detonation, and the oscillation then decreased. These research results can serve a basis for reducing tunnel blasting over-excavation under this condition and optimizing blasting parameters.

1. Introduction

With the rapid development of the national economy of China, the smooth blasting technology of rock mass has been widely used in underground engineering, water conservancy and hydropower, mining, and other fields and thus has produced substantial economic and social benefits [1, 2]. However, in the blasting construction of underground projects, such as tunnels, the over-excavation phenomenon is still prominent, increases construction costs, and threatens the safety of tunnel construction. Through field research, we found that when the design contour line is exposed with a gentle dip crack (small gap between the crack and the peripheral hole), the over-excavation phenomenon is difficult to avoid. Therefore, studying the propagation pattern of blasting cracks under the condition of cracks with gentle dip angles between boreholes is of significant importance. The knowledge of the interaction between blasting cracks and existing joints under the action of explosive loads informs the smooth blasting technique in tunneling practice. Dynamic crack propagation under blast loading has always been a widely studied topic in dynamic fracture mechanics research. Many researchers have proposed and adopted many testing techniques, such as dynamic photo elasticity, dynamic moire, and holographic interferometry [3, 4]. However, the dynamic photo elastic optical fringes in the strain singular region at the crack tip are dense, and the mechanical information of the singular stress region at the crack tip cannot be obtained directly. The caustics method was first proposed by Manogg [5] to solve mechanical and optical singularity. The Greek scholar Theocaris [6] used this method to determine the plastic zone size, crack tip position, and stress intensity factor near the crack tip. Kalthoff et al. [7] extended this method to the field of dynamic fracture mechanics. Yang et al. [8, 9] used dynamic caustic testing to simulate the blasting process of a defective rock mass, studied the law of crack propagation under blasting with a precrack collinear blasting hole, and examined the influence

of nonfilling and intermittent filling joints on the crack propagation law and the mechanism of crack propagation under fracture control blasting of slotted charge. Yuan [10] studied the fracturing mechanism of shock wave interactions between two adjacent blast holes in deep rock blasting. Wang et al. [11] studied the dynamic mechanical behavior of the main crack in the blasting of two grooving blast holes and the secondary crack propagation derived from the tip of a prefabricated defect. Yang and Ding et al. [12] included crack and void defects into the same research system from an experimental point of view and further studied the effect of defects on the crack propagation of directional fracture-controlled blasting.

The expansion of the main crack and the derivation crack generated by the tip of a defect medium under the action of the loading and attenuation of the explosion stress wave and the explosive gas is complicated under blasting load. The role of stress wave and detonation gas in crack propagation has been extensively studied; however, the stress field formed is complex due to their mutual influence and different contributions in rock blasting. Thus, a unified understanding has not been achieved. Scholars have analyzed the dynamic crack propagation process under the simultaneous blasting of two holes by applying different techniques. Holloway [13] used dynamic holographic interferometry to study the characteristic fringes of crack propagation displacement and analyzed the crack propagation displacement peak region. Zhang [14] adopted marble as the research object and studied the crack initiation, expansion, and convergence under two-hole simultaneous detonation condition through dynamic photoelastic testing. Huang [15] et al. used rheological element numerical analysis to simulate the rock fracture process under double-hole blasting, obtained the crack propagation form, and explored the entire block breaking and blasting funnel formation processes under impact load. Yang [16, 17] and Yue [18] conducted experiment with organic glass plate (PMMA) and used three different grooving models to study the dynamic crack propagation of double-hole simultaneous blasting and determined the crack tip propagation speed, acceleration, stress intensity factor, and energy release rate. Wang [19] performed two-hole simultaneous blasting tests under prefabricated horizontal and vertical defect models through dynamic caustics testing and obtained the variation trends of the crack propagation path, propagation velocity, angle, acceleration, and stress intensity factor. Li [20] obtained the propagation law of the main crack and the crack derived from the tip of a double vertical prefabricated crack under the condition of simultaneous initiation of two holes in the slit charge with different charge quantities.

The law of crack propagation under the action of single-hole blasting with defective media has been extensively studied. Theoretical bases and experimental ideas corresponding to simultaneous blasting with two holes for the dynamic response of cracks in models without defects and in those with horizontal and vertical defects have been provided, thereby establishing a foundation for subsequent research. However, the dynamic propagation of cracks in models with inclined defects has not been studied in detail. The current study focuses on the problem of gentle dip cracks existing in tunnel blasting. The influence of prefabricated cracks with gentle dip angles on the dynamic propagation of cracks is studied and analyzed under the condition of simultaneous blasting with two holes by conducting a dynamic caustic test. The propagation path, failure pattern, crack propagation velocity, and stress intensity factor of cracks derived from the tip of prefabricated cracks and the main crack of explosion are determined. This work aims to (1) address the blasting effect of tunnel blasting under the condition of gently inclined cracks and (2) provide theoretical support for the optimization of blasting parameters during tunnel construction.

2. Digital Laser Dynamic Caustics Test System

2.1. Test Principle. The caustics method [21] transforms the complex deformation state of the stress concentration area in the medium to be measured into a simple and clear shadow optical figure by using the mapping relation of geometrical optics. A caustics image schematic diagram is shown in Figure 1.

The thickness of the area near the crack tip and the refractive index of the material change regularly when a plane transparent specimen with a crack is subjected to load. Under the irradiation of a beam satisfying certain conditions, dark spots (caustic speckles) and bright lines (caustic lines) appear in the area near the crack tip. The size of the plastic zone near the crack tip, the location of the crack tip, and stress intensity factor can be determined by their morphological characteristics. The dynamic caustics test system of the explosive loading digital laser aims to visually display the stress distribution in the specimen in accordance with changes in the optical properties of the specimen. The dynamic changes in deformation and stress are recorded with a high-speed photography system.

2.2. Test System. The new digital laser dynamic focal line test system [22] is composed of a laser, a beam expander, a loading frame, a field mirror combination, a high-speed camera, a synchronous switch, and a computer, as shown in Figure 2. The beam expander and field lens I process the high-brightness light wave continuously emitted by the laser into parallel light incident to the surface of the specimen. The specimen in the destruction stage deflects the parallel light, and the deflected light beam is polymerized at high speed through field lens II. The camera lens can capture the moving focal line image at a certain moment, and the entire crack propagation can be recorded by adjusting the exposure speed of the camera.

2.2.1. High-Speed Photography System. A Fastcam-SA5 (16G) high-speed digital color camera with "long/short focal-length lenses" is used in the experiment. The shooting area, image resolution, and recording time can be adjusted by changing the number of frames. The corresponding performance and technical parameters are shown in Table 1.

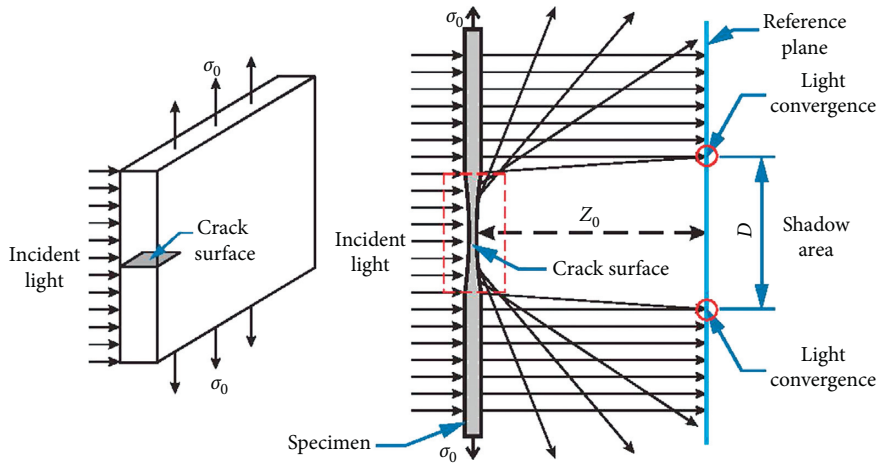

Figure 1: Schematic diagram of focal line imaging.

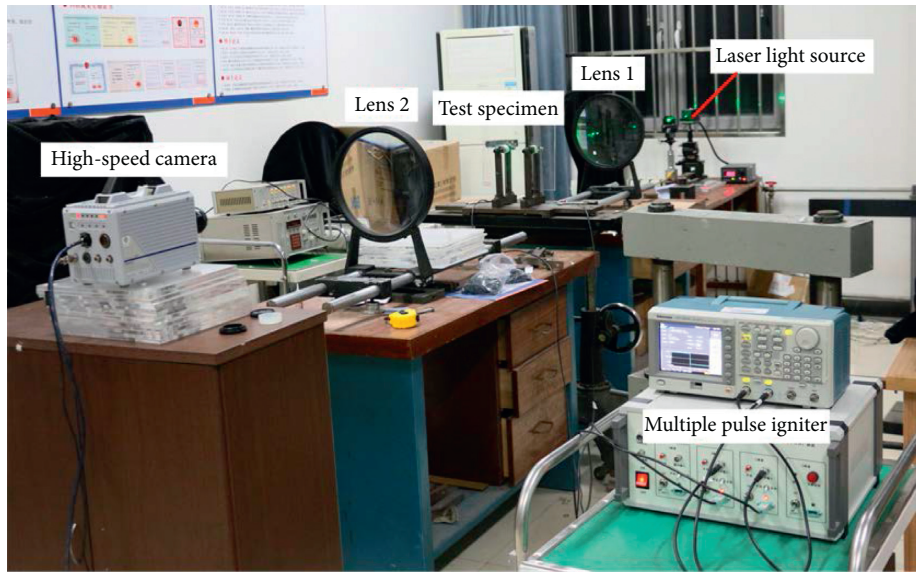

Figure 2: New digital laser dynamic caustics test system.

Table 1: Performance and technical parameters of the high-speed camera.

Frame number (fps)	Shooting interval (μs)	Maximum exposure speed (μs)	Resolution (pixels)
1000	1000	1	1024 × 1024
5000	200	1	1024 × 1024
10000	100	1	1024 × 744
50000	20	1	512 × 272
70000	14.2	1	320 × 272
87500	11.4	1	320 × 224
100000	10	1	390 × 192

The high-speed camera has a short exposure time and thus can fulfill the shooting requirements in the blasting process with extremely short duration. Moreover, the camera has a signal output-input port, which can be connected to a computer to easily complete the performance debugging, image information acquisition, and preliminary data processing of the high-speed camera with a software system.

2.2.2. Test Light Source. The laser is excited using the principle of stimulated radiation, which amplifies or oscillates light in certain excited materials. The monochromatic laser has the advantages of high brightness, strong directivity, and good coherence; thus, wavelength changes will not affect other optical characteristics, such as the refractive index. The test system uses a LWGL300-1500 mW laser as the light source. This laser is easy to install, has a stable

performance, and emits a laser wavelength of 532 nm. Consequently, it can achieve optimal matching with the sensitivity of high-speed cameras and can provide sufficient light intensity in an extremely short time to meet the requirements of high-speed cameras during shooting.

2.2.3. Detonation and Explosive Devices. The explosive used in this test is lead azide (PbN_6). The drug pack containing the PbN_6 element was placed in a prefabricated blast hole to control the uncoupling coefficient, and the signal and detonating lines were extended from the blast hole. The detonating line was connected to the detonating device, and a program was used to control the multichannel pulse igniter to induce the explosive. The detonating device could control the multiburst detonation time and realized the blasting test under various conditions. The signal line was connected to the external signal input port of the camera to enhance the precision of the explosion loading control and to improve the accuracy and objectivity of the recording effect of the explosion process.

3. Test Specimen Preparation and Parameter Determination

3.1. Preparation of Specimens. The cracking propagation characteristics of PMMA under the blast load are similar to those of rock materials [18, 23], and it has a high caustic optical constant which can produce a clear caustic curve and is widely used in photometric mechanical tests. The dynamic mechanical parameters of the PMMA plate are shown in Table 2.

This experiment was conducted at the State Key Laboratory of Geotechnical Mechanics and Underground Engineering, China University of Mining and Technology. The blast-hole spacing in the specimen size is based on previous research results, which is under the condition of 12–15 cm blast-hole spacing, the explosion of lead azide explosives can achieve the expansion and connection of blast cracks. On the other hand, the number and expansion form of the main cracks on the outside of the blast hole are clearly observed. 90 mm space is reserved on the outside of the blast hole, so the sample size is selected as 300 mm. So, a PMMA plate sized 300 mm × 300 mm (length × width) was used as the test material. The plate thickness is 5 mm [23], the diameter of the two blast holes is 10 mm, and the distance between the two blast holes is the same as that from the boundary of the specimen. A prefabricated slit with a width of 1 mm is cut by using the laser between the two holes, and the length is 70 mm. The angle between the prefabricated crack and the horizontal line is 30°. Three groups of experiments were designed to control the angle of prefabricated cracks and the position between the two boreholes. The prefabricated cracks in specimen C are located in the geometric center position between the two boreholes (the vertical distance between the left and right boreholes is 30 mm). The vertical distances between the prefabricated crack position and the right borehole in specimen A and B are 25 and 20 mm, respectively, and the vertical distances between the prefabricated crack position and the left borehole are 35 and 40 mm, respectively. The dimension parameters of each specimen are shown in Figure 3.

According to previous research on the quasi-static mechanism of detonation gases of uncoupled charge [24], when the uncoupled coefficient is 1.67, the distance between the charge and the borehole wall exhibits a considerable buffer effect on explosion, and the amplitude of stress wave itself is reduced. At this time, the ultimate length of crack propagation is the largest, and the role of detonation gas is the most evident.

An uncoupled charge with uncoupled groove and uncoupled coefficient controlled to 1.67 is used to study the evolution and interaction of cracks and the penetration form between boreholes under the action of explosive gas, maximize the crack growth length, and eliminate the disturbance of stress wave propagation and explosive gas flow caused by shaped charge blasting [25]. The charge was implemented through the following steps. First, one end of the blast hole is sealed with hard transparent tape. Second, a small amount of super glue is applied on the edge of a medicine tube (inner diameter 5 mm and outer diameter 6 mm), which is then placed into the blast hole and affixed on the hard transparent glue. Third, the safety film is introduced into the medicine tube with an appropriately sized glass rod and spread along the inner wall of the medicine tube to ensure that the plastic wrap is fixed with the hard transparent adhesive. The flatness of the cling film and the presence or absence of air bubbles are checked, and any excess cling film around the blast hole is trimmed. Fourth, 120 mg PbN_6 elemental explosive is placed in the medicine tube, the blast hole is blocked, the wire is connected, and the two ends of the blast hole are clamped with a rubber band clamp to complete the uncoupled closed charge.

The PMMA with explosives was placed on the specimen clamp. The blast-hole wire was connected to the igniter and clamped with a fixture to adjust the relative position of the light source, specimen, and lens until the high-speed camera can capture a clear image. The high-speed camera was set to shoot the number of frames in accordance with the size of the desired shooting range. The test was affected by factors such as the sizes of the specimen and the field of view. The camera shooting speed was set to 100000 frames (photo acquisition time difference is 10 μs). After all the object positions are determined, the multipulse igniter was activated by a computer detonation program, and the two blast holes are simultaneously detonated. Finally, a photograph of the focal spot was captured at each moment during the blasting failure of the specimen.

3.2. Calculation of Sample Failure Parameters

3.2.1. Calculation of Crack Motion Characteristics. The crack tip is at the center of the focal speckle. At the same resolution, the displacement vector and direction of the crack tip can be determined at a certain time by the high-speed photography system.

When the interval between two adjacent photographs is small enough, the crack propagation speed and acceleration can be calculated by using the following formula:

Table 2: Dynamic mechanical parameters of PMMA plates.

Mechanical parameters	C_p (P-wave propagation velocity)	C_s (S-wave propagation velocity)	E_d (modulus of elasticity)	μ_d (Poisson ratio)	$_C$ (optical parameter)
Numerical value	2320 m/s	1260 m/s	6.1 GN/m^2	0.31	85 μm^2/N

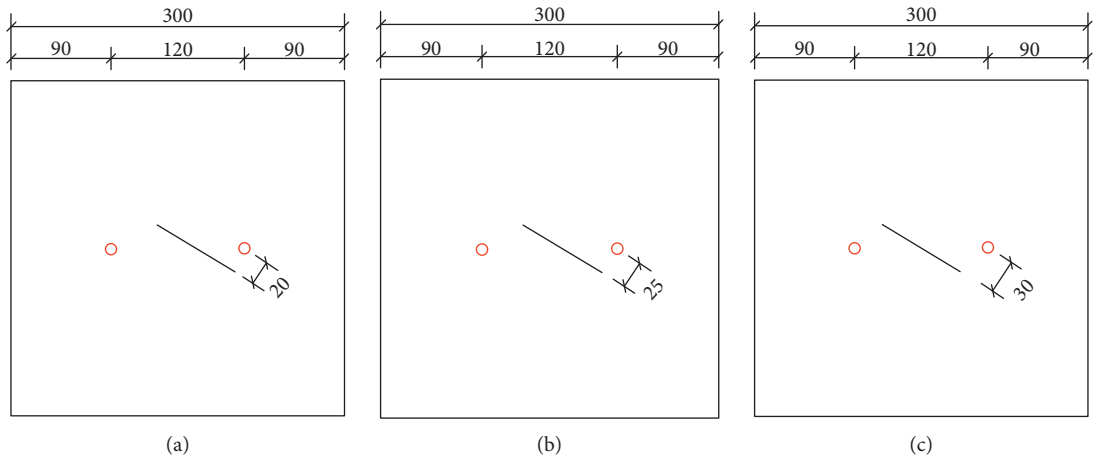

Figure 3: Diagram of dimension parameters of test specimens (mm): (a) specimen A, (b) specimen B, and (c) specimen C.

$$\left.\begin{aligned} v(t) &= \lim_{\Delta t \longrightarrow 0} \frac{x(t+\Delta t) - x(t)}{\Delta t} = \frac{\Delta x}{\Delta t} \\ a(t) &= \lim_{\Delta t \longrightarrow 0} \frac{v(t+\Delta t) - v(t)}{\Delta t} = \frac{\Delta v}{\Delta t} \end{aligned}\right\}, \quad (1)$$

where Δx is the displacement of the crack tip of two consecutive photos, Δv is the amount of change in speed during the shooting interval, and Δt is the high-speed camera shooting interval.

3.2.2. Calculation of Dynamic Stress Intensity Factor at Crack Tip. After the explosion, the explosion pressure pulse in the explosion stress field mainly propagates in the form of compression and shear waves. Therefore, normal and shear stresses are generated at any point inside the medium. Consequently, the explosive stress field is mostly compounded, and the crack generated in the medium is mostly compounded crack. For the dynamic caustics test, the test principle can express the compounded stress intensity factor at the crack tip as follows [25]:

$$\left.\begin{aligned} K_{\mathrm{I}}^d &= \frac{2\sqrt{2\pi}\, F(v)}{3 Z_0 d_e |c| g^{5/2}} D_{\max}^{5/2} \\ K_{\mathrm{II}}^d &= \mu K_{\mathrm{I}}^d \end{aligned}\right\}, \quad (2)$$

where K_{I}^d and K_{II}^d are the dynamic stress intensity factors of type I and type II cracks, respectively, at the crack tip of the composite type

$D_{\max}$ is the maximum diameter of the focal spot of the compounded crack tip

Z_0 is the distance from the reference plane to the plane of the object (900 mm in this test)

c is the stress optical constant of the material; $c = 0.88 \times 10^{-10}$ m^2/N

d_e is the effective thickness of the sample; for transparent materials, the effective thickness of the material is its actual thickness

μ is the stress intensity factor proportional coefficient, which can be obtained from the curve relationship between the maximum and minimum diameters of the focal spot

$F(v)$ is the correction factor caused by the crack propagation speed, and its value is approximately equal to 1 at a practical crack propagation speed

4. Test Results and Analysis

4.1. Analysis of Explosion Crack Propagation Form. Photographs of the damaged pieces of each specimen are shown in Figure 4. After the explosion, a crushing zone with a diameter of approximately 30 mm is formed around the blast hole under the action of the blasting load, and the periphery of the blast hole is extended with cracks of different lengths. New secondary cracks are also derived from both ends of the prefabricated crack. For discussion, the long new crack that extends the radial direction of the blast hole is called the main crack, and the new secondary crack at both ends of the prefabricated crack is called the derivative crack. After the explosion, 4-5 radial main cracks are generated around each blast hole and symmetrically distributed in pairs (cracks I-I′ and II-II′ in the figure). The angular relationship between the main crack and the central prefabricated crack shows that the cracking direction of the

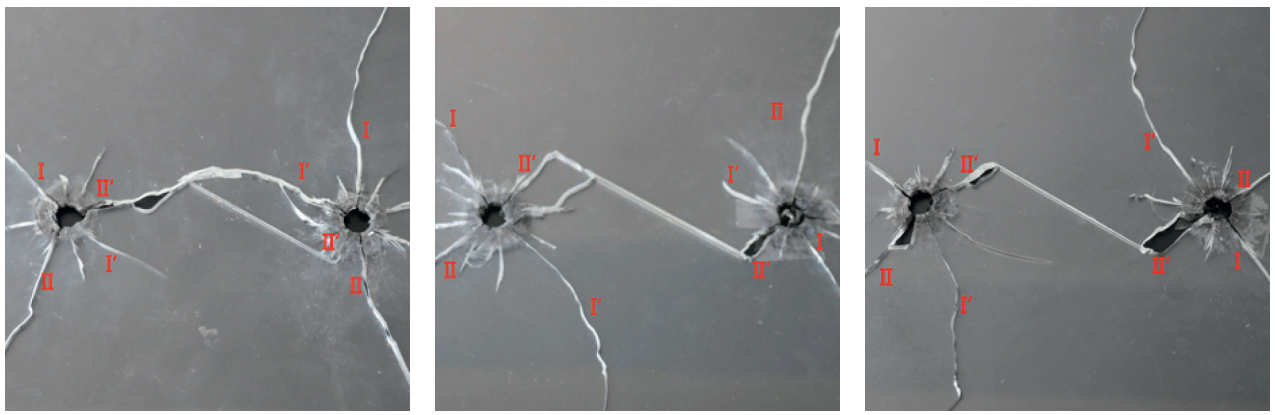

(a) (b) (c)

Figure 4: Photographs of each specimen after destruction: (a) specimen A, (b) specimen B, and (c) specimen C.

main crack I-I is nearly parallel to the prefabricated crack, the direction of the main crack II-II intersects with the prefabricated crack at a large angle, and the main cracks of the two groups are approximately vertical.

Outside of the two blast holes, the formed main cracks I and II extend toward the free surface in the form of a near-straight line or a large radius curve, thus showing an explosion crack propagation pattern in a homogeneous medium. The extension is long because it is guided by the free surface, and the extended path has no defect interference. Most of the cracks are finally perpendicular to the free surface, and the expansion mode is relatively simple. This study mainly analyzes the interwell crack penetration mode affected by the prefabricated cracks and thus focuses on analyzing the extended modes of main cracks I and II. Figure 4 indicates that the extended form of the main crack between the two blast holes has the following characteristics. (1) Guided by the prefabricated cracks between the two blast holes, main crack II of each blast hole expands along the direction of the blast hole and the prefabricated crack tip and finally interacts with the derivative crack at the tip of the prefabricated crack. (2) Main crack I is cracked in a direction nearly parallel to the prefabricated crack, but the expansion form differs due to the different distance between the prefabricated crack and the blast hole. For specimen C, main crack I′ is not affected by the prefabricated crack after the cracking and extends in the boundary direction after the cracking because the prefabricated crack is at the geometric center position between the two blast holes. When the vertical distance of the prefabricated fissure from one of the blast holes decreases, its guiding effect on main crack I′ becomes increasingly apparent. For specimen A, the main crack of the proximal blast hole (right blast hole) is generated and deflected toward the prefabricated crack by the "drag" of the distal end of the prefabricated crack; finally, it penetrates the distal end of the prefabricated crack.

This group of experiments simulates the blasting effect when a gentle dip joint exists between the surrounding holes of the tunnel. When the explosive explodes, it is guided by the existing joints; the crack is preferentially extended to the direction of the minimum resistance line and connects with the existing joints. At this time, the fracture morphology of the rock between the holes is no longer along the direction of the line of the blast hole (Figure 5).

As shown in the figure, when the existing joint is near the midpoint of the connection of the two blast holes (specimens C and B), the final failure mode of the rock mass is represented by the "*Z*" shape of the blast hole along the direction of the minimum resistance line and the existing joints. When the existing joint is adjacent to one of the blast holes (specimen A), its guiding effect on the crack and the "drag" effect are significantly enhanced. The main cracks of the explosion are all extended to the existing joint direction, and a complex stress field is generated between the adjacent blast hole and the existing joint. Under the action of the reflection stress wave, the rock mass breaks and falls off, leading to over-excavation.

4.2. Analysis of Dynamic Focal Spot Variation during Explosion. High-speed photographic acquisition of the focal spot during the whole explosion is performed to accurately determine the position of the crack tip at different times, and Figures 6–11 show the image of the focal spot of each specimen at different times.

The currently accepted blasting theory believes that the damage of the medium under blasting load is the result of the interaction of the explosive stress wave and the explosive gas. Combining this theory and the results of the dynamic caustics test, we can divide the damage of the specimen into two stages.

In the focal speckle photos at different moments, there will be obvious wave fronts in the action stage of the explosion stress wave, and it will gradually spread over time. At this time, the location of the focal speckles is only near the blast hole, indicating that the burst cracks are generated but not extended. In the blasting gas phase, the wavefront of the stress wave in the figure disappears, and the focal speckles begin to shift significantly, indicating that the crack propagation phase is mainly driven by the blasting gas at this time.

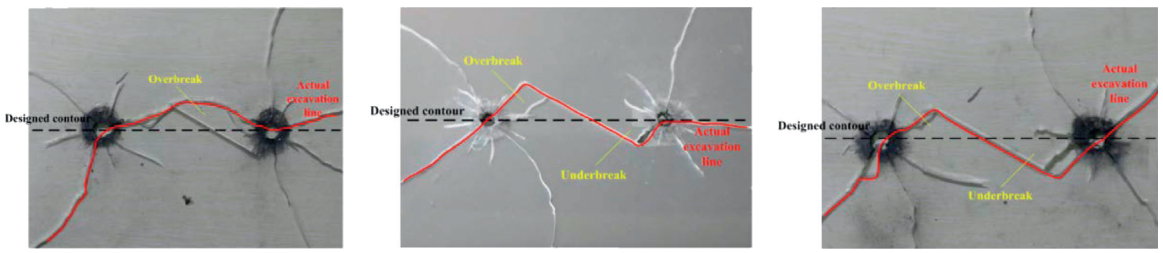

(a) (b) (c)

Figure 5: Final damage form of each specimen: (a) specimen A, (b) specimen B, and (c) specimen C.

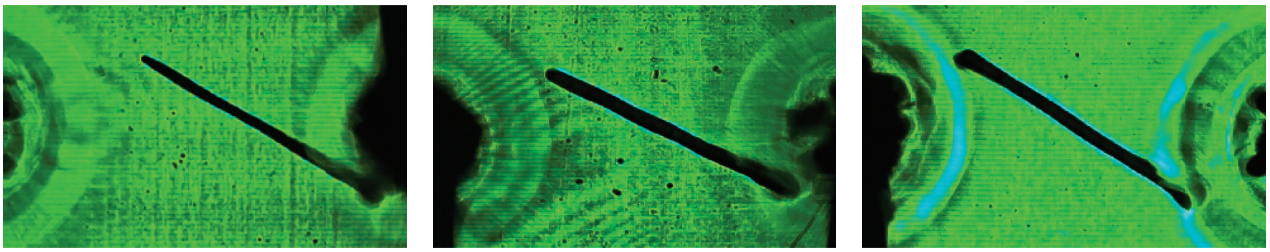

(a) (b) (c)

Figure 6: Photograph of focal spot of each specimen after 10 μs of detonation: (a) specimen A, (b) specimen B, and (c) specimen C.

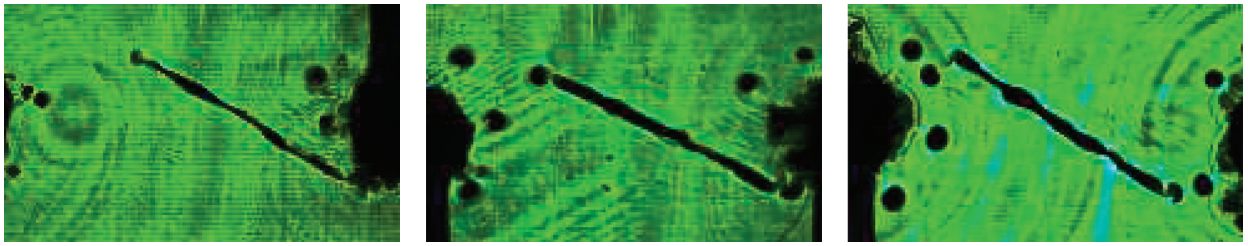

(a) (b) (c)

Figure 7: Photograph of focal spot of each specimen after 30 μs of detonation: (a) specimen A, (b) specimen B, and (c) specimen C.

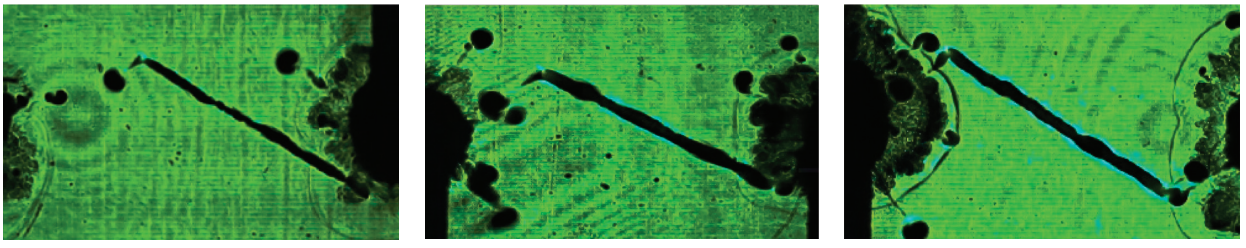

(a) (b) (c)

Figure 8: Photograph of focal spot of each specimen after 50 μs of detonation: (a) specimen A, (b) specimen B, and (c) specimen C.

4.2.1. First Stage: Crack Initiation under the Action of Explosive Stress Wave

(1) A crush zone is formed around the blast hole after the explosives are detonated. Figure 6 shows that when the explosive is detonated at 10 μs, the explosive stress wave propagates to the tip end of the crack, and the medium around the hole is crushed to form a large dark area. For specimens A and B, the tip end of the crack is deformed under the action of the explosion stress wave because the prefabricated crack is not at the geometric center between the blast holes. At this time, the stress wave is reflected, significant energy accumulation and stress concentration occur near the tip end of the crack, and a dark region (an unformed focal spot) is formed. For specimen C, given that

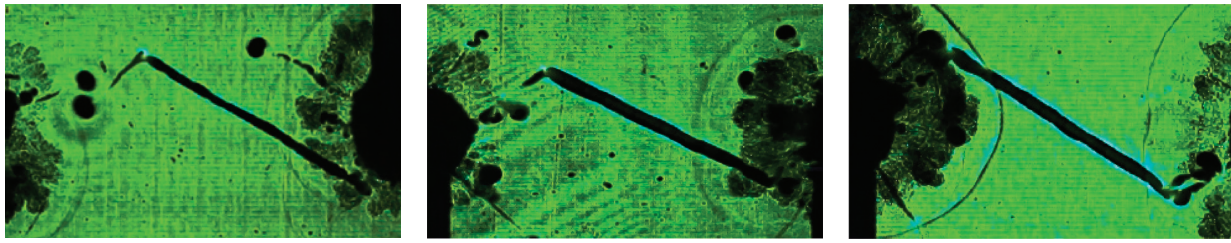

(a) (b) (c)

Figure 9: Photograph of focal spot of each specimen after 70 μs of detonation: (a) specimen A, (b) specimen B, and (c) specimen C.

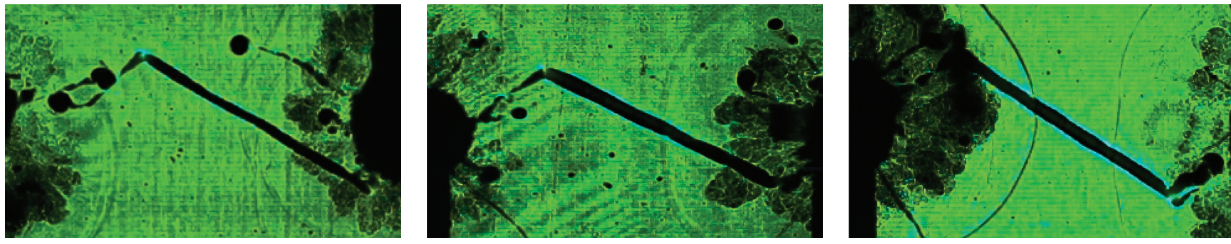

(a) (b) (c)

Figure 10: Photograph of focal spot of each specimen after 90 μs of detonation: (a) specimen A, (b) specimen B, and (c) specimen C.

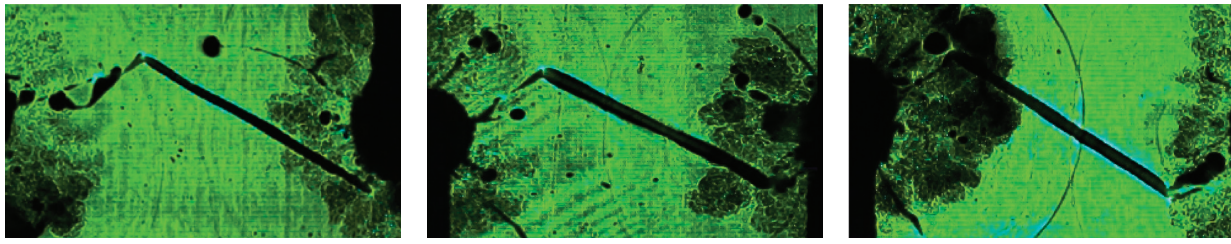

(a) (b) (c)

Figure 11: Photograph of focal spot of each specimen after 120 μs of detonation: (a) specimen A, (b) specimen B, and (c) specimen C.

the prefabricated crack is at the geometric center between the blast holes, the stress wave generated by the explosion of the two blast-hole explosives simultaneously reaches the tip end of the crack to form a symmetrical dark region. At this stage, the focal spot is not formed, the explosive stress wave is weakened by the material impedance, and its energy is not enough to extend the prefabricated crack.

(2) The explosion stress wave continues to propagate, and the radial crack of the blast hole is formed. Figure 7 indicates that when the explosive is detonated for 30 μs, the explosion stress waves of the two blast holes reach the geometric center position between the blast holes. The prefabricated cracks undergo significant deformation under the action of the stress waves, and the reflection and refraction of the stress waves become increasingly evident. Meanwhile, many focal spot images are formed around the blast hole, which indicate the formation of the main crack under the action of the explosion stress wave. From the distribution of focal speckles, every blast hole forms approximately two to three focal speckles in the field of view, all of which are radially distributed around the blast hole. For specimens A and B, the focal spot formed by the proximal blast hole and the near-vertical direction of the prefabricated crack reaches the tip end of the prefabricated crack due to the geometric position of the prefabricated crack. An unformed focal spot appears at the distal tip, indicating that the explosive stress wave has propagated along the prefabricated crack to the distal tip position. For specimen C, the stress waves generated by the explosion of the two blast-hole explosives reach the center position of the prefabricated crack simultaneously; the focal spot is formed at both ends of the prefabricated crack and tends to move toward the adjacent blast hole.

4.2.2. Second Stage: Main Crack Growth under the Action of Explosive Gas

(3) The explosive gas begins to wedge into the crack, and the main crack is formed. Figure 8 shows that when the explosive is detonated for 50 μs, the effect of the explosion

stress wave is remarkably weakened, and the explosive gas begins to wedge into the crack. The focal spot near each blast hole begins to move significantly, and the crack begins to expand. As shown in the figure, the movement of each focal spot near the blast hole is nearly linear and follows two distinct dominant directions, namely, a near-parallel direction with the prefabricated crevice and toward the proximal end of the prefabricated crevice. Therefore, the existence of prefabricated cracks has a significant guiding effect on the explosion crack. The type I crack initiation characteristics are noticeable, and the focal spot is enlarged. For specimen A, the focal spot at the right end of the prefabricated crack begins to move toward the right blast hole, indicating that the explosive gas has wedged into the prefabricated crack and caused it to crack. For specimen B, the tip focal spot on the left side of the prefabricated crack starts to move toward the left blast hole, meets the main crack of the left blast hole, and causes a hook phenomenon, indicating that the two cracks are nearly through. For specimen C, the tip focal spot at both ends of the prefabricated crack moves toward the adjacent blast hole simultaneously and meets the main crack of the blast hole; the crack is nearly continuous.

(4) The main crack of the explosion is connected with the prefabricated crack. Figures 9–11 indicate that when the explosive is detonated for 70 μs, the right crack of the prefabricated crack of specimen A and the main crack of the right blast hole are connected. In addition, for specimen A, the main blast hole main crack I′ of specimen A starts to deflect toward the right end of the prefabricated crack when the explosive is detonated for 90 μs because the prefabricated crack position is not at the geometric center between the blast holes. Therefore, when the crack between the two blast holes is not centered, the prefabricated crack exerts a "drag" effect on the explosion crack parallel to it. In addition to this crack, other cracks at this stage continue to expand under the driving of the explosive gas. The direction of the explosion crack outside of the two blast holes is along the boundary direction of the nearest specimen and finally penetrates perpendicularly to the boundary. The free boundary has a significant guiding effect on the crack propagation direction (Figure 4).

4.3. Analysis of Crack Propagation Velocity of the Main Crack. The view of the test field selects the area between the two blast holes to reveal the perforation form of prefabricated and explosion cracks between the holes under double-hole blasting conditions. According to the final destruction form of each specimen in Figure 4, the main cracks between the blast holes are mainly I and II cracks generated by the explosive detonated of each blast hole. The location of the crack tip can be determined in accordance with the center of the caustic speckle. Thus, the law of crack propagation can be analyzed on the basis of the moving speed of the caustic speckle. The instantaneous velocity of the focal spot motion in the next photograph can be replaced by the average velocity in the two adjacent photographs by the difference method because of the small interval between the high-speed cameras. On this basis, the growth velocity curves of the main cracks are plotted in Figure 12.

Figure 12 reveals that the propagation velocity of the main crack of each specimen increases to the peak velocity rapidly in a relatively short time and then decreases. Most of the cracks eventually reach or approach zero. A comparison of the crack propagation time of each specimen shows that the crack propagation time of each of the main blasting cracks is basically the same between specimens A and B because the prefabricated crack is at the geometric center position between the blast holes, and the main crack propagation times of specimens A and B are different. The prefabricated crack of specimen A has a large difference between the two blast holes. Thus, the extension time of main crack II′ from the blast hole to the prefabricated crack tip is considerable varied. The right blast hole is closest to the prefabricated crevice. Therefore, the main rupture of the right blast hole II′ penetrates the prefabricated crevice in a short time after the explosive is detonated, and its peak velocity is 660.73 m/s. By contrast, the left blast hole main crack II′ shows two peak velocities during the expansion process. After the explosive is detonated, the main crack II′ of the left blast hole is affected by the explosion stress wave to reach the first peak velocity of 515.44 m/s at 30 μs. Then, the expansion speed decreases slightly as the stress wave intensity decreases. After the explosive is detonated for 50 μs, the explosive gas plays a leading role in crack propagation; the crack propagation speed increases again and reaches the second peak velocity of 535.49 m/s at 70 μs, after which the fluctuation reduces to the prefabricated crack. For specimen B, given the small difference between the prefabricated crack and the distance between the two blast holes, the relationship between the expansion speed of the main crack II′ generated by the two blast holes and the detonation time is similar to that of specimen C, which is in the explosive detonation 20–30 μs. It reaches a peak velocity after, declines rapidly, and reduces to 0 within 60 μs, showing the significantly dominant characteristic of the explosive stress wave.

The expansion process of the main crack I of each specimen is relatively complicated. The cracking direction of the main crack I of each blast hole is nearly parallel to the prefabricated cracks (such as the main crack of specimen B's left blast hole and specimen C's double blast hole I). When the crack propagation trajectory is deflected outside the field of view, it shows that the expansion time is short. During this time period, the blast stress wave plays a leading role in its expansion and the crack propagation speed appears to be a slow decline after reaching the peak speed in a short time (20–30 μs). Meanwhile, when the crack tip reaches the edge of the field of view, the propagation process is unfinished. Thus, the propagation speed is not zero. For specimen A's double blast hole and specimen B's right blast hole main crack I, the extended velocity-time curve has two distinct peak speeds due to the interaction of the explosive stress wave and the explosive gas during the expansion process. The first peak velocity is reached within a short time of detonation (approximately 20 μs) and then decreases rapidly. When the explosive gas enters the crack, the crack propagation reaches the second peak velocity due to the gas

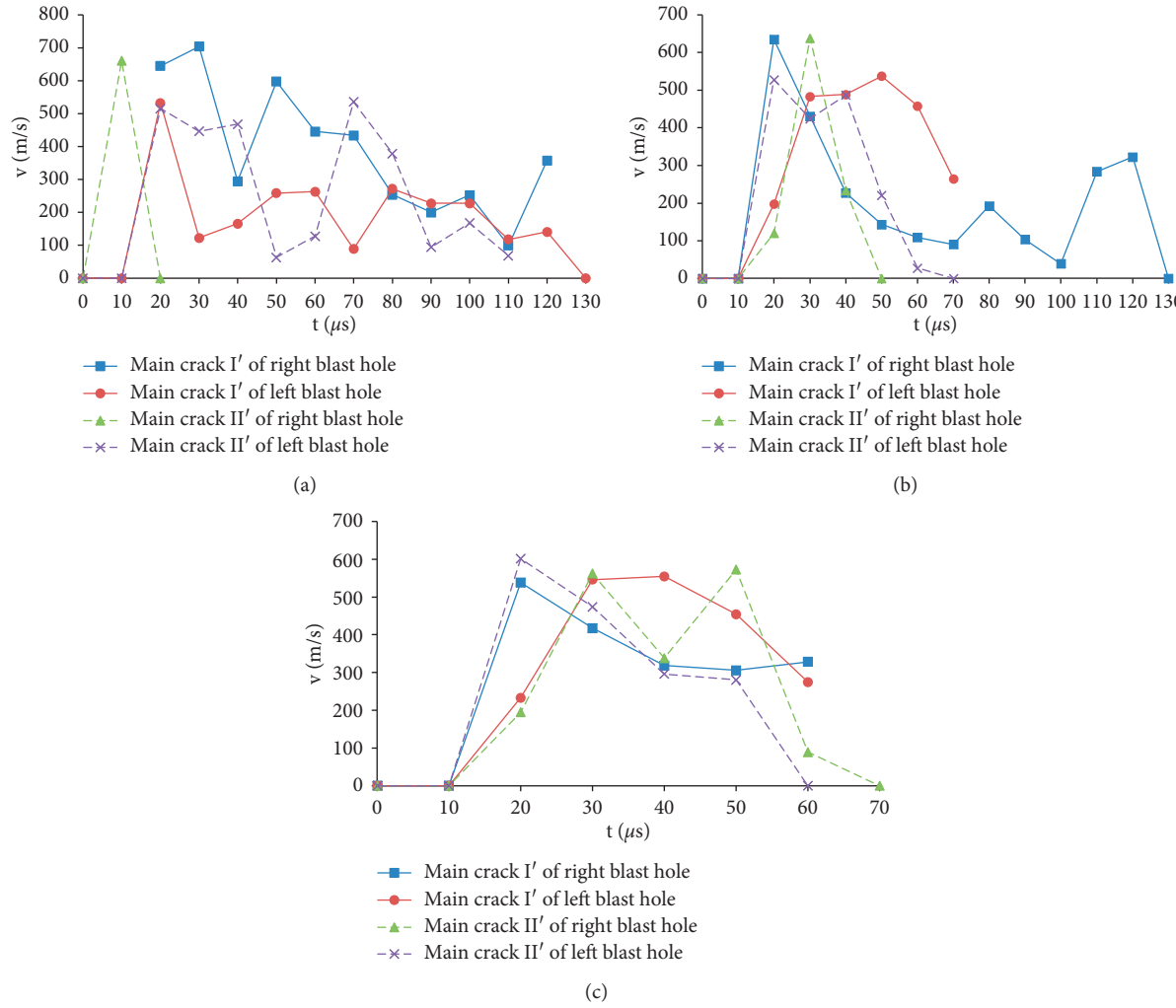

Figure 12: Curve of the relationship between the crack propagation velocity and the detonation time of each specimen: (a) specimen A, (b) specimen B, and (c) specimen C.

wedge effect. Then, the fluctuation decreases except for the fluctuation of the right borehole of specimen A, which is close to the prefabricated crack. Its main crack I penetrates the distal end of the prefabricated crack, and the final velocity is not 0. The other two main cracks have stopped extension (the propagation velocity decreases to 0) with the weakening of the driving effect of the detonation gas.

On the basis of the peak velocity of the main crack of each specimen in Figure 12, the correlation curve with the position of the prefabricated crack is drawn, as shown in Figure 13.

Figure 13 indicates the following. (1) When the prefabricated crack is at the geometric center position between the two blast holes, the stress wave propagation after the explosion of the two blasthole explosives of the same dose and the explosion gas expansion pressure has the same distance for the prefabricated crack. At the same time, the distance between the blast hole and the prefabricated crack tip is relatively long. In this case, the peak velocity of the

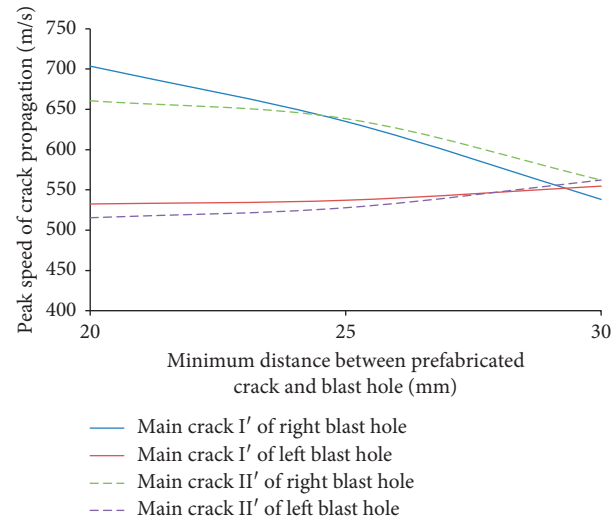

Figure 13: Curve of the peak velocity of the main crack propagation of the specimen and the position of the prefabricated crack.

main crack propagation is mainly dominated by the instantaneous blast stress wave. In a short time (20–30 μs), the surrounding medium of the blast hole is similar in nature to the homogeneous medium; thus, the peak velocity of the four main cracks' propagation is basically the same. (2) For specimens A and B, the prefabricated crack direction is close to the right-side blast hole, and the tip end exerts an evident "drag" effect on the expansion of the main blast hole crack. At this time, the two main crack peak expansion speed of right blast hole is significantly larger than that of the left blast hole. (3) Under the influence of the prefabricated crack tip on the "drag" effect of the proximal blast-hole crack, the peak velocity of crack propagation of each blaster decreases as the distance between the prefabricated crevice and the blast hole increases (the main blast hole main cracks I and II in Figure 13). However, when the distance between the two increases to a certain value, the "drag" effect is weakened, and the peak velocity increase of the crack propagation is small (the left blast holes I′ and II′ in Figure 13).

4.4. Analysis of Stress Characteristics at the Tip of the Blasting Main Crack. The stress intensity factor reflects the strength of the stress field at the crack tip. The eigenvalue is substituted into formula (2) by measuring the diameter of the focal spot. The stress intensity factor at the crack tip is calculated, and the stress at the crack tip during crack propagation is analyzed. The variation of the field and the stress intensity factor of the main crack tip of each specimen change with time, as shown in Figure 14.

The figure shows that the stress intensity factor of each specimen shows a trend of increasing first and then decreasing with time, which is mainly related to the loading and unloading action of the stress wave. For specimen C, the model is symmetrical, and the stress intensity factor of the main crack tip of the two blast holes has the same change trend because the prefabricated crack is at the geometric center of the specimen. The entire expansion process of the crack is affected by the explosion stress wave, and the tensile damage shows a type I crack. After explosion, the complex stress field appears at the crack tip under the loading of the explosive stress wave, and the stress intensity factor thus increases instantaneously. At 30 μs, the stress intensity factors at the main crack tip of the left and right boreholes reach their peak values simultaneously, namely, 1131.81 and 1033.47 kN/m$^{3/2}$, respectively. Afterward, the effect of the explosion stress wave is weakened, and the stress intensity factor of each crack tip begins to decrease until cracks stop growing. The entire expansion process reflects the loading of the crack tip by the stress wave and the accumulation and release of energy at the crack tip. Then, with the stress wave unloading, the stress intensity factor begins to decrease. For specimens A and B, the prefabricated crack position is close to the right blast hole. Thus, the extension time of the main crack II of the right blast hole is very short, and the tip stress intensity factor reaches the peak quickly after the detonation, which are1090.43 and 1055.42 kN/m$^{3/2}$, respectively, and then decreases rapidly. A big difference exists in the variation of the stress intensity factor at the tip of the main crack of the left blast hole of the two specimens, and this discrepancy is mainly related to the position of the prefabricated crack. For specimen A, because the left blast hole is far away from the prefabricated cracks, the explosive energy is concentrated between the right blast hole and the prefabricated crack tip. Therefore, the II tip stress field complexity of the main blast hole burst is more complicated low, and the stress intensity factor is small. However, at approximately 50 μs, the prefabricated crack tip-derivative crack interacts with the main crack II. Under the action of the reflected tensile wave, the tip stress field becomes complex, and the stress intensity factor reaches a peak of 801.10 kN/m$^{3/2}$ and then decreases slowly. For specimen B, the difference between the prefabricated crack and the distance between the two blast holes are similar. The main crack II of the blast hole on the left side and the II tip stress intensity factor of the main crack of the right blast hole show a similar evolution law, that is, increasing to a peak value of 1209.55 kN/m$^{3/2}$ under the action of explosive stress wave loading and then decreasing under stress wave unloading. The crack is propagated at the tip of the prefabricated crack at 60 μs, and the stress field becomes complicated. Consequently, the stress intensity factor reaches the second peak (1023.24 kN/m$^{3/2}$) and then decreases under the action of the detonation gas.

For the main crack I on the outer side of the blast hole, the stress intensity factors at the crack tip of each specimen are quite different. For specimen C, because of its geometrically symmetrical structure, the stress intensity factor of the main crack "I" in the left and right blast holes exhibits the same evolution law as that of the blasting crack "II," which increases to the peak values of 911.59 and 889.70 kN/m$^{3/2}$ under the loading of explosive stress wave and then decreases gradually under the unloading of the explosive stress wave. For specimens A and B, given that the prefabricated crack is close to the right blast hole, after the explosion, the energy gathers at the crack tip of the right blast hole first. The stress intensity factor at the tip of the main crack of the blast hole on the right side of the two specimens reaches a peak rapidly under the action of the explosive stress wave loading, which are 1072.54 and 616.94 kN/m$^{3/2}$, respectively. Then, it decreases rapidly with the attenuation of the explosive stress wave. However, under the effect of subsequent explosion gas expansion pressure, the "I" tip stress intensity factors of the main cracks of the two specimens reach the second peak at 40 and 60 μs, respectively, which are 1036.40 and 836.74 kN/m$^{3/2}$, respectively, and then fluctuate downward under the action of the explosion gas expansion pressure. The stress concentration at the tip of the main crack in the left blast hole of the two specimens is weak. Thus, the peak of the stress intensity factors of the two specimens is low overall. The peak values are 269.95 and 339.94 kN/m$^{3/2}$, respectively. For both cases, the explosive stress wave loading increases to peak value at the initial stage of explosion and then decreases gradually.

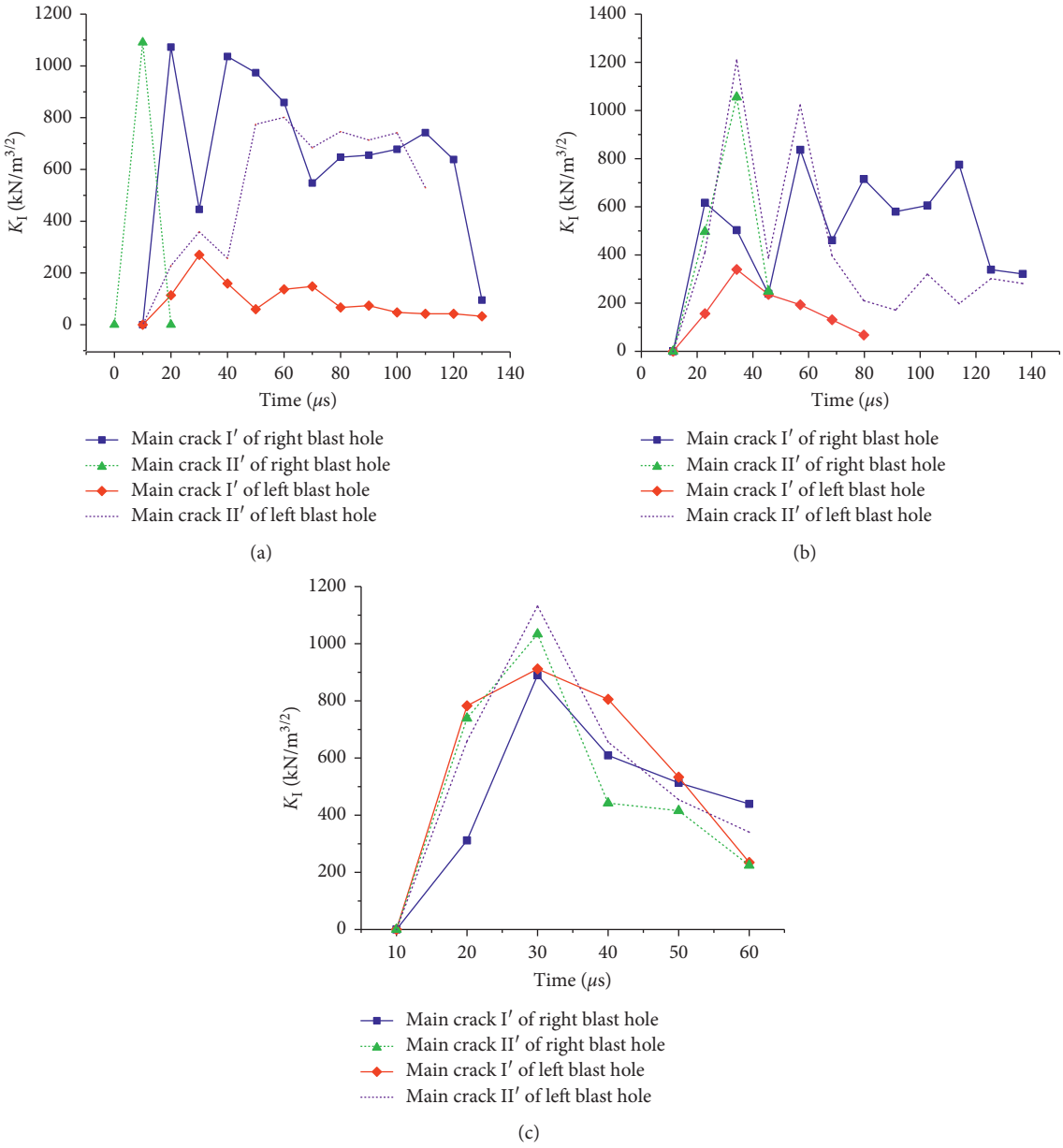

Figure 14: Curve of stress intensity factor at crack tip: (a) specimen A, (b) specimen B, and (c) specimen C.

5. Conclusions

(1) Combined with the results of laboratory tests and numerical simulations, when a gentle dip crack exists between the two blast holes, the main crack between the holes is preferentially extended to the vertical direction of the blast hole and the crack and penetrates the prefabricated crack. The final blasting effect is "*Z*"-type over-under excavation.

(2) According to the evolutionary law of caustic speckle in dynamic caustics testing, two groups of near-vertical main cracks are generated along the borehole radial direction under the action of explosive stress wave after explosion. Then, under the action of the explosion gas expansion pressure, the main crack between the holes preferentially expands along the vertical direction of the blast hole and the crack and finally forms a fracture surface with the crack.

(3) After explosion, the propagation velocity of the main crack of explosion reaches its peak instantaneously during the loading process of the explosive stress wave. Then, with a decrease in the attenuation oscillation of the stress wave, the peak propagation velocity of each main crack decreases with an increase in the vertical distance between the borehole and the crack.

(4) After explosion, the stress field at the tip of the explosion crack becomes complicated and the stress intensity factor of the crack tip of each explosion peaks due to the reflection and tensile action of the explosion stress wave. However, the peak value

shows a remarkable difference due to the varied vertical distances between the crack and each blast hole. Then, the stress wave action weakens, and the oscillation of the stress intensity factor at the crack tip decreases during the unloading process until it penetrates the crack.

Data Availability

The data used to support the findings of this study are available from the first author upon request.

Conflicts of Interest

The authors declare that they have no conflicts of interest.

Acknowledgments

This work was supported by the National Natural Science Foundation of China (nos. 41502270 and 41702300).

References

[1] H. Li, X. Li, J. Li, X. Xia, and X. Wang, "Application of coupled analysis methods for prediction of blast-induced dominant vibration frequency," *Earthquake Engineering and Engineering Vibration*, vol. 15, no. 1, pp. 153–162, 2016.

[2] P. Yan, W. Lu, J. Zhang, Y. Zou, and M. Chen, "Evaluation of human response to blasting vibration from excavation of a large scale rock slope: a case study," *Earthquake Engineering and Engineering Vibration*, vol. 16, no. 2, pp. 435–446, 2017.

[3] H. P. Rossmanith and A. Shukla, "Dynamic photoelastic investigation of interaction of stress waves with running cracks," *Experimental Mechanics*, vol. 21, pp. 415–420, 1981.

[4] W. H. Wilson, "An experimental and theoretical analysis of stress wave and gas pressure effects in bench blasting" Ph.D thesis, University of Maryland, College Park, MD, USA, 1987.

[5] X. Su and Z. Lei, "Experimental method of dynamic caustics and its application in fracture mechanics," *Acta Mechanica Sinica*, vol. 3, no. 2, pp. 160–172, 1987.

[6] P. S. Theocaris, "Local yielding around a crack tip in plexiglas," *Journal of Applied Mechanics*, vol. 37, no. 2, pp. 409–415, 1970.

[7] J. F. Kalthoff, "Shadow optical analysis of dynamic shear fracture," *Spie Photomechanics & Speckle Metrology*, vol. 27, no. 10, pp. 835–840, 1988.

[8] R. Yang, L. Yang, Z. Yue et al., "Dynamic caustics experiment of crack propagation in material containing flaws under blasting load," *Journal of China Coal Society*, vol. 34, no. 2, pp. 187–192, 2009.

[9] R. Yang, Z. Yue, J. Dong et al., "Dynamic caustics experiment of blasting crack propagation in discontinuous jointed material," *Journal of China University of Mining & Technology*, vol. 37, no. 4, pp. 467–472, 2008.

[10] W. Yuan, S. Liu, W. Wang et al., "Numerical study on the fracturing mechanism of shock wave interactions between two adjacent blast holes in deep rock blasting," *Earthquake Engineering and Engineering Vibration*, vol. 18, no. 4, pp. 735–746, 2019.

[11] Y. Wang, R. Yang, C. Ding et al., "Dynamic caustics experiment on crack propagation of defective medium under the effect of explosive stress waves of double holes," *Journal of China Coal Society*, vol. 41, no. 7, pp. 1755–1761, 2016.

[12] R. Yang, C. Ding, L. Yang et al., "Experimental study on controlled directional fracture blasting on PMMA mediums with flaws," *Chinese Journal of Rock Mechanics and Engineering*, vol. 36, no. 3, pp. 690–696, 2017.

[13] D. C. Holloway, "Application of holographic interferometry to stress wave and crack propagation problems," *Optical Engineering*, vol. 21, no. 5, pp. 769–792, 1982.

[14] Z. Zhang, *Directional Fracture Controlled Blasting*, China Metallurgical Industry Press, Beijing, China, 2000.

[15] T. Huang, P. Chen, G. Zhang et al., "Numerical simulation of two-hole blasting using numerical manifold method," *Explosion and Shock Waves*, vol. 26, no. 5, pp. 434–440, 2006.

[16] R. Yang, Y. Wang, Z. Yue et al., "Dynamic behaviors of crack propagation in directional fracture blasting with two holes," *Explosion and Shock Waves*, vol. 33, no. 6, pp. 631–637, 2013.

[17] R. Yang, Y. Wang, H. Xue et al., "Dynamic behavior analysis of perforated crack propagation in two-hole blasting," *Procedia Earth & Planetary Science*, vol. 5, pp. 254–261, 2012.

[18] Z. W. Yue, L. Y. Yang, and Y. B. Wang, "Experimental study of crack propagation in polymethyl methacrylate material with double holes under the directional controlled blasting," *Fatigue & Fracture of Engineering Materials & Structures*, vol. 36, no. 8, pp. 827–833, 2013.

[19] Y. Wang, Y. Shang, Z. Shi et al., "Dynamic caustics experiment on crack propagation in defective medium by directional breaking with double hole blasting," *Blasting*, vol. 1, no. 1, 2018.

[20] L. I. Qing, Q. Yu, G. Zhu et al., "Experimental study of crack propagation under two-hole slotted cartridge blasting with different amounts of charge," *Chinese Journal of Rock Mechanics and Engineering*, vol. 36, no. 9, pp. 2205–2212, 2017.

[21] L. Yang, R. Yang, Z. Yue et al., "Experimental system of digital laser dynamic caustics," China Patent: 201120458198.X, 2012.

[22] L. Yang, R. Yang, and P. Xu, "Caustics method combined with laser & digital high-speed camera and its applications," *Journal of China University of Mining & Technology*, vol. 42, no. 2, pp. 188–194, 2013.

[23] R. Yang, P. Xu, L. Yang et al., "Dynamic caustic experiment on fracture behaviors of flawed material induced by pre-notched blasting," *Explosion and Shock Waves*, vol. 36, no. 2, pp. 145–151, 2016.

[24] Y. Wang, "Study on the mechanism of rock crushing under dynamic-static effect in the explosion and dynamic crack propagation" Ph.D thesis, China University of Mining & Technology, Beijing, China, 2016.

[25] S. Shen, W. Liao, and Y. Xuet al., "Dynamic caustics test of rock mass under different joint spacing conditions with two-hole blasting," *Journal of China Coal Society*, vol. 43, no. 8, pp. 2180–2186, 2018.